A&A 467, 283–294 (2007)
DOI: 10.1051/0004-6361:20066375

Astronomy & Astrophysics

Detailed chemical composition of Galactic Cepheids

A determination of the Galactic abundance gradient in the 8–12 kpc region⋆

B. Lemasle[1,2], P. François[3,2], G. Bono[4,5], M. Mottini[5], F. Primas[5], and M. Romaniello[5]

[1] Université de Picardie Jules Verne, Faculté des Sciences, 33 rue Saint-Leu, 80039 Amiens Cedex 1, France
[2] Observatoire de Paris-Meudon, GEPI, 92195 Meudon Cedex, France
e-mail: Bertrand.Lemasle@etud.u-picardie.fr
[3] European Southern Observatory (ESO), 3107 Alonso de Cordova, Vitacura, Casilla 19001, Santiago 19, Chile
[4] INAF-Osservatorio Astronomico di Roma, via Frascati 33, 00040 Monte Porzio Catone, Italy
[5] European Southern Observatory (ESO), Karl-Schwarzschild-Strasse 2, 85748 Garching bei Muenchen, Germany

Received 11 September 2006 / Accepted 10 January 2007

ABSTRACT

Aims. The recent introduction of high-resolution/large spectral-range spectrographs has provided the opportunity to investigate the chemical composition of classical Cepheids in detail. This paper focusses on new abundance determinations for iron and 6 light metals (O, Na, Mg, Al, Si, Ca) in 30 Galactic Cepheids. We also give a new estimate of the Galactic radial abundance gradient.
Methods. The stellar effective temperatures were determined using the method of line depth ratios, and the surface gravity and the microturbulent velocity v_t by imposing the ionization balance between Fe I and Fe II with the help of curves of growth. Abundances were calculated with classical LTE atmosphere models.
Results. Abundances were obtained with rms accuracies of about 0.05–0.10 dex for Fe, and 0.05–0.20 dex for the other elements. Cepheids in our sample have solar-like abundances, and current measurements agree quite well with previous determinations. We computed "single zone" Galactic radial abundance gradients for the 8–12 kpc region and found a slope for iron of –0.061 dex kpc^{-1}.

Key words. stars: abundances – stars: supergiants – Galaxy: abundances – Galaxy: evolution

1. Introduction

Galactic abundance gradients are one of the most important inputs for the numerical models of the chemical evolution of Galactic disks. Different stellar tracers have been used to estimate the gradient, namely planetary nebulae, giant stars, old open clusters, HII regions, and young, *B*-type main sequence stars. If the existence of the gradient is now widely accepted, its precise value still needs to be established.

As a matter of fact, empirical estimates give quite steep gradients for iron ranging from –0.05 dex kpc^{-1} to –0.07 dex kpc^{-1}: see, e.g., Friel et al. (2002) who found a slope of –0.06 dex kpc^{-1}; Kovtyukh et al. (2005), who obtained a gradient of –0.06 dex kpc^{-1}; and Luck et al. (2006), who estimated a slope of –0.068 dex kpc^{-1} using classical Cepheids as chemical tracers. However, much shallower slopes have also been estimated: –0.023 dex kpc^{-1} by Twarog et al. (1997), –0.044 dex kpc^{-1} by Andrievsky et al. (2004). And in a few cases the gradient was not detected: –0.017 dex kpc^{-1} by Neese & Yoss (1988) and –0.003 dex kpc^{-1} by Kilian-Montenbruck et al. (1994). The broad range of empirical radial gradients also applies to the other light metals adopted in current investigations. Thorough reviews of gradient values for many elements can be found for example in Andrievsky et al. (2002a) and Chiappini et al. (2001).

Beyond an expected scatter due to measurement errors, these discrepancies between steep and shallow slopes of the Galactic radial abundance gradient might trace its evolution as a function of stellar ages. This working hypothesis has been suggested in several studies (Friel et al. 2002; Maciel et al. 2003) based either on planetary nebulae or on open clusters. From this point of view, Cepheids are young Galactic objects that trace the present-day abundance gradient, and only a few elements (C, N, Na, and perhaps Mg and Al); (Kovtyukh et al. 1996) may have their abundances modified during the life of the Cepheids, while all the others should trace the abundance pattern as it was at the birth of the star.

Compared to other methods, the use of classical Cepheids offers many advantages because these stars

- are excellent distance indicators;
- are luminous enough and provide the opportunity of determining the gradient over a significant fraction of the Galactic disk;
- allow the measurements of many elements that cannot be investigated with other stellar tracers;
- show spectra with many absorption lines and, in turn, reliable abundance values.

An extension of the available data is mandatory for constraining the slope of the Galactic abundance gradients on a more quantitative basis. This paper is the first in a series focussed on accurate and homogeneous abundance measurements for a good sample of Galactic Cepheids. The sample includes objects that are in common with previous studies, but current spectra typically present a higher spectral resolution and/or a wider spectral range.

⋆ Based on observations made with the 1.52 m ESO Telescope at La Silla, Chile.

Table 1. Observations: date, exposure time, and S/N at 600 nm.

Object	date	exposure time (s)	S/N
AD Pup	02/01/01	600	65
AH Vel	29/12/00	300	111
...	31/12/00	100	88
AP Pup	30/12/00	500	119
...	31/12/00	300	105
...	01/01/01	300	114
...	02/01/01	120	53
AQ Car	02/01/01	240	76
AQ Pup	01/01/01	500	84
AT Pup	30/12/00	600	73
AX Vel	31/12/00	400	94
BG Vel	30/12/00	600	100
BN Pup	02/01/01	600	62
DR Vel	01/01/01	600	95
lCar	29/12/00	180	42
...	30/12/00	120	41
...	31/12/00	80	40
...	01/01/01	120	37
MY Pup	31/12/00	100	94
RS Pup	31/12/00	240	48
RY CMa	29/12/00	240	84
...	30/12/00	600	67
RY Vel	29/12/00	600	69
RZ CMa	02/01/01	600	77
RZ Vel	01/01/01	300	42
ST Vel	02/01/01	600	80
SW Vel	31/12/00	500	153
SX Vel	31/12/00	400	82
T Vel	31/12/00	400	106
TW CMa	02/01/01	600	66
UX Car	31/12/00	400	105
V397 Car	02/01/01	300	86
V Car	29/12/00	600	78
V Vel	31/12/00	300	136
VX Pup	02/01/00	300	77
VY Car	31/12/00	240	130
VZ Pup	01/01/01	600	55
WX Pup	01/01/01	300	53

2. Observations

The observations were performed in 2002 at the 1.52 m ESO telescope in La Silla. We collected 38 high-resolution spectra of Galactic Cepheids with the fibre-fed Extended Range Optical Spectrograph (FEROS), with a resolving power of 48 000 and a spectral range spanning from 370 to 920 nm. The spectra were reduced using the FEROS package within MIDAS. The S/N ratio at 600 nm ranges from 40 to 136 (see Table 1).

3. Methodology

The determination of an accurate temperature is a critical point in the abundance determination. In this investigation, the temperature was derived spectroscopically and does not rely on photometric indices.

3.1. Line list

For iron, we used the line list proposed by Mottini et al. (2007), which contains 246 Fe I lines and 17 Fe II lines covering a wide spectral range corresponding to the FEROS one. These lines are a compilation of the line lists from Clementini et al. (1995), Fry & Carney (1997), Kiss & Vinko (2000) and Andrievsky et al. (2002a). They were completed with a selection of lines from VALD (Vienne Atomic Line Database) (Kupka et al. 1999; Ryabchikova et al. 1999), picked for effective temperatures corresponding to Cepheids: 4500–6500 K.

Mottini et al. devised the following approach to removing blended lines.

- All the lines stored in VALD between 4800 and 7900 Å and corresponding to Cepheids typical parameters have been compiled.
- This compilation was over-plotted onto the iron lines, with special attention given to the lines located within ±3 Å of an iron line.
- If the these lines contributed to more than 5% of the iron line strength, then the iron line was neglected.

This test was performed on three observed spectra for Cepheids with effective temperatures about 4500 K, 5500 K, and 6500 K. It might remain a few slightly blended lines, since a few weak lines may not be listed in VALD, but their overall contribution is negligible.

The same method was adopted to clean the line list of alpha elements, which are much less numerous: 4 lines for *AlI*, 9 lines for *MgI*, 4 lines for *NaI*, 2 lines for *OI*, 20 lines for *CaI* and 24 lines for *SiI*. For all the lines, the physical properties (oscillator strength, excitation potential) listed in VALD were adopted.

3.2. Equivalent widths

The measurement of equivalent widths (EW) was performed with a semi-interactive code (*fitline*) developed by P. François. This code is based on genetic algorithms from Charbonneau (1995), and it mimics the way genetic mutations affect DNA, driving the evolution of species. Lines are fitted by a Gaussian defined by four parameters: central wavelength, width and depth of the line, and the continuum value. Line after line, the algorithm runs in the following way:

1. An initial set of Gaussians is computed, giving random values to the four parameters.
2. The quality of each fit is estimated by calculating the χ^2.
3. A new "generation" of Gaussians is calculated from the 20 best fits after adding random modifications to the initial set of parameters values ("mutations").
4. The new set replaces the old one, and its accuracy is estimated by once again using a χ^2 evaluation.
5. The process is iterated 100 to 200 times until the convergence to the best Gaussian fit is attained.

In the current investigation we limit our analysis to weak, non blended lines, all of which could be fitted by a Gaussian. The strong lines were neglected. Some weak but asymmetric lines were also neglected. This selection reduced the number of lines really used to 30–90 for FeI, 5–10 for FeII, 1–3 for O, Na, Mg and Al, 1–10 for Ca, and 10–20 for Si.

3.3. Temperature determination

We obtained the stellar effective temperature $T_{\rm eff}$ by using the method of line depth ratios, described in Kovtyukh & Gorlova (2000). This method only relies on spectroscopy and, therefore, is independent of interstellar reddening. The key advantage to

Table 2. Atmospheric parameters of the Cepheid sample with periods from Fernie's database (Fernie et al. 1995).

Object	P	phase	$T_{\rm eff}$	$\log g$	$V_{\rm t}$	[Fe/H]
	d		K		km s^{-1}	dex
AD Pup	13.594	0.406	5290 ± 146	1.0	2.4	–0.4
AH Vel	4.227171	0.408	6080 ± 80	1.5	3.5	–0.1
...	4.227171	0.887	6483 ± 168	1.6	3.2	–0.1
AP Pup	5.084274	0.733	6180 ± 84	2.2	4.0	–0.2
...	5.084274	0.926	6148 ± 93	1.7	3.5	–0.2
...	5.084274	0.130	5723 ± 87	1.6	3.7	–0.2
...	5.084274	0.329	5557 ± 86	1.7	3.5	–0.2
AQ Car	9.76896	0.528	5374 ± 104	0.5	3.5	–0.1
AQ Pup	30.104	0.309	5304 ± 133	0.3	3.3	–0.4
AT Pup	6.664879	0.594	5348 ± 144	0.7	3.2	–0.4
AX Vel	3.6731	0.598	5995 ± 161	1.8	3.2	–0.3
BG Vel	6.923655	0.895	5957 ± 111	1.5	3.5	–0.2
BN Pup	13.6731	0.116	5615 ± 81	1.0	3.0	–0.1
DR Vel	11.1993	0.179	5183 ± 87	0.5	3.0	–0.2
lCar	35.551341	0.234	4885 ± 87	0.7	3.5	0.1
...	35.551341	0.262	4848 ± 91	0.5	3.5	0.1
...	35.551341	0.290	4900 ± 105	0.5	3.5	0.1
...	35.551341	0.318	4821 ± 87	0.6	3.2	0.1
MY Pup	5.695309	0.904	6114 ± 110	1.4	2.8	–0.25
RS Pup	41.3876	0.826	5056 ± 110	0.2	3.2	–0.1
RY CMa	4.67825	0.257	5666 ± 131	1.2	3.0	–0.2
...	4.67825	0.473	5460 ± 106	1.2	3.2	–0.1
RY Vel	28.1357	0.424	5124 ± 149	0.3	3.5	–0.3
RZ CMa	4.254832	0.084	5800 ± 186	1.0	2.7	–0.3
RZ Vel	20.39824	0.606	4992 ± 131	0.5	3.2	–0.1
ST Vel	5.858425	0.224	5474 ± 109	1.1	3.2	–0.1
SW Vel	23.441	0.583	5150 ± 96	0.5	5.0	–0.2
SX Vel	9.54993	0.983	6248 ± 132	1.3	2.8	–0.2
T Vel	4.639819	0.135	5800 ± 91	1.8	3.0	–0.1
TW CMa	6.99507	0.471	5364 ± 184	1.0	4.0	–0.5
UX Car	3.682246	0.577	6002 ± 97	1.7	3.5	–0.1
V397 Car	2.0635	0.765	5959 ± 161	1.5	3.5	–0.15
V Car	6.696672	0.357	5423 ± 112	1.0	3.0	–0.1
V Vel	4.371043	0.279	5608 ± 121	1.3	3.0	–0.3
VX Pup	3.01087	0.733	5870 ± 97	1.8	3.0	–0.15
VY Car	18.913762	0.334	6127 ± 147	1.5	4.2	–0.05
VZ Pup	23.171	0.653	5015 ± 114	0.2	4.0	–0.3
WX Pup	8.93705	0.497	5263 ± 132	0.7	3.0	–0.1

this approach is that it uses weak, neutral metallic lines appropriately selected:

- The excitation potentials of line depth ratios must differ as much as possible for a good estimation of $T_{\rm eff}$, but lines should be relatively weak to limit the dependence on microturbulent velocity.
- Pairs of lines must be close enough to eliminate errors in continuum placement.
- Ionized lines are excluded because they are too sensitive to the surface gravity.
- The line depth ratios are based on weak lines, and thus metallicity effects on temperature determination are strongly moderated. It is worth noting that two lines located on different parts of the curve of growth do not have the same behaviour when metallicity changes.

Kovtyukh & Gorlova (2000) proposed 32 analytical relations for determining $T_{\rm eff}$ from the line depth ratios. After measuring the line depths and calculating subsequent ratios, we obtained 32 temperatures whose mean value gave us the stellar temperatures listed in Table 2. According to the quoted authors, the uncertainties on absolute temperatures are of the order of 80 K, and uncertainties on relative temperatures inside a sample are smaller and of the order of 10–15 K.

3.4. Atmospheric parameters

The surface gravity, $\log g$, and the microturbulent velocity $v_{\rm t}$ are determined by imposing the ionization balance between Fe I and Fe II with the help of the curves of growth. Lines of the same element in different ionization states should give the same abundance value. Iterations on the values of $\log g$ and $v_{\rm t}$ are repeated until Fe I and Fe II adjust to the same curve of growth. Figures 1 and 2 show the curves of growth for Fe I and Fe II in AP Pup. An independent support to the $T_{\rm eff}$ value is given by the evidence that both high and low $\chi_{\rm ex}$ lines properly fit the curve of growth. Once abundances were calculated, atmospheric parameters were checked and in particular, the Fe I abundances depend neither on line strength nor on excitation potential. The atmospheric parameters for the target Cepheids are listed in Table 2.

3.5. Abundance determination

Abundances are then calculated with the help of the atmospheric model of Spite (1967) based on the grid of models of Gustafsson et al. (1975). These models are based on the following assumptions: plane-parallel stratification, hydrostatic equilibrium, and LTE. The abundance determination codes adjust abundances until matching the observed equivalent width. We adopted the

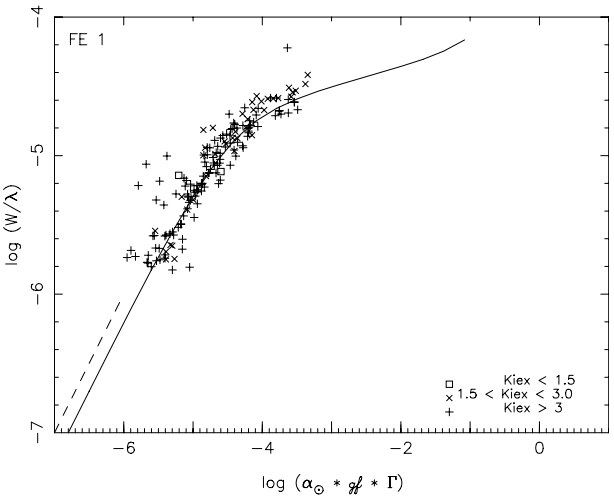

Fig. 1. Observed curve of growth for Fe I in APPup. The full line is the theoretical curve of growth for a typical line (λ = 5000 Å, χ_{ex} = 3). The atmospheric parameters adopted for this star are T_{eff} = 6180 K, $\log g$ = 2.2, v_t = 4.0 km s^{-1}, and [Fe/H] = –0.2 dex. The dashed line on the left shows the [Fe/H] = 0 location.

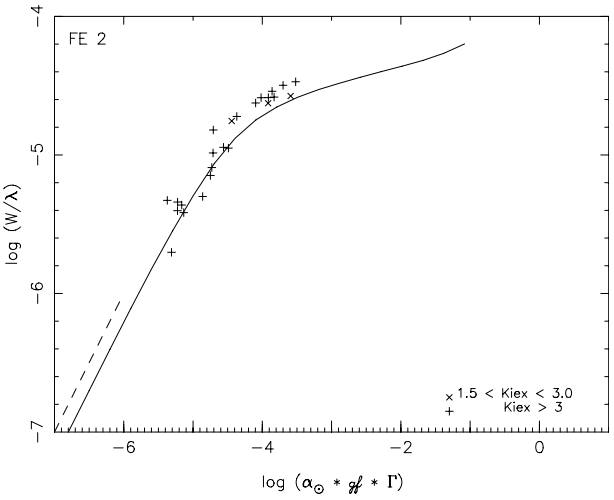

Fig. 2. Observed curve of growth for Fe II in APPup. The full line is the theoretical curve of growth for a typical line (λ = 5000 Å, χ_{ex} = 3). The atmospheric parameters adopted for this star are T_{eff} = 6180 K, $\log g$ = 2.2, v_t = 4.0 km s^{-1}, and [Fe/H] = –0.2 dex. The dashed line on the left shows the [Fe/H] = 0 location.

scaled-solar chemical abundances suggested by Grevesse et al. (1996).

For every star in the sample, the final abundance was obtained by calculating the mean value of the abundances found for each line. The use of a substantial number of "clean" lines drives to very small error bars, which are less than 0.10 dex for most of them. Oxygen and aluminum abundances were checked with synthetic spectra, to account for the occurrence of blended lines. In most cases, the influence of the blended lines was negligible. In a few cases, abundances were modified, but the change never exceeded 0.1 dex.

3.6. Uncertainties in abundance determinations

The first source of uncertainty comes from the extraction of data from the spectra: the equivalent width and the continuum placement (which influences the measure of the equivalent width) must be precisely determined. To minimize the errors, we limited our analysis to symmetric and unblended lines and neglected the most crowded parts of the spectra in selecting the line list. We only adopted weak or relatively weak lines ($EW \leq 120$ mÅ) and assumed they could be fitted by Gaussians.

The second crucial point is to have precise temperature determinations, because this intrinsic parameter strongly affects the line strength. We used, as mentioned above, the calibration relations from Kovtyukh & Gorlova (2000). According to these authors, the uncertainties on absolute temperatures are at most ≈80 K. Since current spectra have been secured with a spectral resolution of only 48 000, the intrinsic dispersion in temperature values is on average ≈80−130 K.

In order to constrain how the uncertainties affect abundance determinations, we finally computed abundances by adopting over or under-estimated values of the atmospheric parameters. The test was carried out with AP Pup, one of our spectra with the lowest S/N (S/N = 53). As expected, only errors on temperature had a noticeable effect: an error of 100 K on the effective temperature implies a difference of about 0.1 dex on abundances values, while errors on surface gravity of $\Delta \log g = \pm 0.3$ and on turbulent velocity of $\Delta v_t \pm 0.5$ km s^{-1} cause much smaller differences, namely 0.02 and 0.05 dex.

Finally, the LTE assumption in the atmosphere models might not be appropriate for supergiant stars, hence the adopted stellar atmosphere models could provide abundance determinations affected by deceptive systematic errors. This effect should be minimized, however, by the fact that we only adopted weak or relatively weak lines. Moreover, Fry & Carney (1997) show that a canonical spectroscopic approach, using classical LTE atmosphere models, gives reliable abundances for Cepheids. In particular, they noted that LTE analysis of dwarfs and Cepheids located in the same open clusters give, within the errors, the same metallicity. Yong et al. (2006) used the same method (classical LTE models) and examined the difference [TiI/Fe] – [TiII/Fe] to test the influence of NLTE effects. The discrepancy between the two different approaches is –0.07 dex and lies within the measurement uncertainties, thus suggesting that the surface gravities derived from ionization equilibrium of Fe spectra are robust.

3.7. Distances

Distance calculations are based on NIR (J, H, K-band) photometry from Laney & Stobie (1994). For a few objects we adopted NIR photometry from the 2MASS catalogue. The mean magnitude of these objects was estimated using the template light curves provided by Soszyński et al. (2005), together with the V-band amplitude and the epoch of maximum available in the literature. Laney & Stobie (1994) magnitudes have already been un-reddened, while for un-reddening the new data, we first computed the relative absorption in the V-band, $A_V = 3.1\ E(B-V)$, and then according to Cardelli et al. (1989) the absorption in the J, H, and K-band, namely $A_J = 0.28\ A_V$, $A_H = 0.19\ A_V$, and $A_K = 0.114\ A_V$. For individual Cepheids we adopted the reddening values given in the Fernie's database (Fernie et al. 1995).

The Cepheid absolute magnitudes were computed using the NIR period-luminosity (PL) relations recently provided by Persson et al. (2004), together with an LMC distance modulus of 18.50. Pulsation periods are from the Fernie's database (Fernie et al. 1995). The period of Cepheids pulsating in the first overtone were fundamentalized, while we adopted the fundamental period for the double-mode pulsators pulsating simultaneously in the fundamental and in the first overtone. The

PL relations provided by Persson et al. (2004) are based on a large and homogeneous sample of LMC Cepheids, but it can be applied to Galactic Cepheids. Indeed, at NIR wavelengths, the slopes and the zero-points of the PL relation depend very weakly on metallicity (Bono et al. 1999; Persson et al. 2004; Mottini et al. 2007). Moreover, the NIR PL relations present an intrinsic dispersion that is significantly smaller than the dispersion of the optical PL relations. The difference is due to the fact that the former ones are, at fixed period, marginally affected by the intrinsic width in temperature of the instability strip. Cepheid distances based on NIR PL relations are more accurate, when compared with optical ones, because they are also marginally affected by the uncertainties in reddening estimates.

The heliocentric distance d can now be computed:

$d = 10^{0.2(m_X^0 - M_X + 5)}$, where $X = J, H, K$.

The heliocentric distance adopted in the following is the mean value between the three distances in J, H, and $K-$ bands to limit random errors. The Galactocentric distance is finally calculated with the classical formula:

$R_{\rm G} = [R_{\rm G,hel}^2 + (d \cos b)^2 - 2\, R_{\rm G,hel}\, d \cos b \cos l\,]^{1/2}$

where $R_{\rm G,hel}$ is the Galactocentric distance of the Sun, d the heliocentric distance of the Cepheid, while l and b are the Galactic longitude and latitude, listed in the Fernie database (Fernie et al. 1995). We assumed a galactocentric distance of 8.5 kpc for the sun (Kerr & Lynden-Bell 1986; Feast & Whitelock 1997).

The results relative to current Cepheid sample are given in Table 3. Distances based on NIR photometry are compared with distances based on the catalogue of light-curve parameters and distances provided by Berdnikov et al. (2000). In this catalogue, the heliocentric distance was calculated using a period-colour relation and photometric measurements in the optical bands. Results show good agreement for Cepheids near the solar circle and are slightly more discrepant toward the outer disk, where the differences can reach 0.3 kpc and even 0.6 kpc (5%) for AD Pup, the most distant Cepheid in our sample.

Table 3. Cepheids distances from IR photometry ($d_{\rm IR}$) and comparison with the distances computed from Berdnikov et al. (2000) ($d_{\rm B}$).

Object	$d_{\rm IR}$ kpc	$d_{\rm B}$ kpc
AD Pup	11.64	11.03
AH Vel	8.59	8.60
AP Pup	8.81	8.75
AQ Car	8.20	8.18
AQ Pup	10.15	10.02
AT Pup	9.07	8.98
AX Vel	8.75	8.71
BG Vel	8.52	8.51
BN Pup	10.64	10.35
DR Vel	8.62	8.57
lCar	8.40	8.40
MY Pup	8.61	8.62
RS Pup	9.19	9.15
RY CMa	9.41	9.26
RY Vel	8.32	8.31
RZ CMa	9.99	9.60
RZ Vel	8.83	8.79
ST Vel	8.78	8.68
SW Vel	9.06	8.98
SX Vel	8.90	8.84
T Vel	8.66	8.62
TW CMa	10.46	10.22
UX Car	8.25	8.27
V397 Car	8.27	8.27
V Car	8.48	8.47
V Vel	8.44	8.44
VX Pup	9.38	–
VY Car	8.16	8.18
VZ Pup	11.56	11.35
WX Pup	9.98	9.80

4. Cepheid metal abundances

Exhaustive studies of Cepheid chemical compositions are recent after rapidly developing since the introduction of high-resolution, wide spectral-range spectrographs. Precise values of Cepheid abundances are necessary for constraining the metallicity dependence of optical and NIR PL relations and for determining Galactic abundance gradients. This investigation deals with accurate abundances of iron and several light metals for a good sample of Galactic Cepheids. The results are listed in Tables 4 and 5, and for each target we give the abundances and the standard deviations (when more than 1 line was adopted). These tables also include previous abundance measurements when available. The literature abundances come mainly from the systematic investigation by Andrievsky and collaborators who published accurate chemical abundances for a large sample of Galactic Cepheids in a series of papers: Andrievsky et al. (2002a,b,c), Luck et al. (2003), Andrievsky et al. (2004).

Current measurements, when compared with the quoted abundance analyses, present on average slightly better standard deviations. We typically used a smaller number of lines, but their fits have been interactively checked one-by-one. The standard deviations are on average smaller than 0.10 dex for Fe and Na, and they range from 0.05 to 0.20 dex for O, Al, Mg, Si and Ca. As a whole, we found that Cepheids in the solar neighbourhod have solar-like abundances both for iron and α-elements, as expected from previous abundance analyses on Cepheids and supergiants (Luck & Bond 1989; Luck & Lambert 1992; Luck & Wepfer 1995; Andrievsky et al. 2002a,b,c; Luck et al. 2003; Andrievsky et al. 2004; Kovtyukh et al. 2005).

4.1. Iron

For iron (see Table 4), our results show excellent agreement with Andrievsky's, and the discrepancies are typically smaller than 0.10 dex. Larger discrepancies (≈0.2–0.3 dex) have only been found for two targets, namely TW CMa and VZ Pup. Similar discrepancies have also been found for other elements. These differences might be due either to different signal-to-noise spectra or to the adopted atmospheric parameters. However, the curves of growth for these two targets and related tests appear to be very consistent. Figures 3–6 show the results for TW CMa and VZ Pup, respectively. A glance at the data plotted in these figures shows good agreement between the predicted curves of growth and current measurements for both FeI and FeII lines. These distant stars deserve further investigations, as they are quite distant from the Galactic centre, and therefore very useful to firmly constrain the metallicity gradient in the outer zones of the Galaxy.

4.2. Oxygen

The oxygen is slightly deficient, as expected after the investigations by Luck & Lambert (1981, 1985), Luck & Bond (1989), and the theoretical work of Schaller et al. (1992). Current

Table 4. Iron, oxygen, sodium abundances, and comparison with previous abundance analyses: (1) Andrievsky et al. (2002a) and foll. (2) Fry & Carney (1997). (3) Luck & Lambert (1981). (4) Boyarchuk & Lyubimkov (1984). (5) Barrell (1982). (6) Luck & Lambert (1985). (7) Luck & Lambert (1992). (8) Andrievsky et al. (1994). (9) Thévenin (1998). (10) Mottini et al. (2007).

Object	[Fe/H] dex	Others dex	[O/H] dex	Others dex	[Na/H] dex	Others dex
AD Pup	–0.20 ± 0.12	–0.24[1]	–0.09 ± 0.04		0.10 ± 0.03	0.06[1]
AH Vel	–0.06 ± 0.05		0.14		0.31 ± 0.01	
...	–0.03 ± 0.07		–0.01		0.25 ± 0.05	
AP Pup	–0.18 ± 0.08	–0.07[10]	–		0.16 ± 0.01	
...	–0.13 ± 0.07		–		0.05 ± 0.04	
...	–0.16 ± 0.08		–0.29		0.02 ± 0.01	
...	–0.15 ± 0.08		0.08		0.03 ± 0.06	
AQ Car	–0.30 ± 0.10		–		0.16 ± 0.01	
AQ Pup	–0.26 ± 0.03	–0.14[1]; –0.09[10]	–0.27 ± 0.04		0.08	0.09[1]
AT Pup	–0.22 ± 0.10		–		0.21 ± 0.04	
AX Vel	–0.15 ± 0.07	–0.67[5]	–		0.06 ± 0.06	
BG Vel	–0.10 ± 0.08		–		0.16 ± 0.06	
BN Pup	–0.03 ± 0.10	0.01[1]; –0.09[10]	–0.01 ± 0.01	–0.06[1]	0.24 ± 0.03	0.09[1]
DR Vel	–0.01 ± 0.07		–0.41 ± 0.09		0.25	
lCar	0.11 ± 0.07	–0.4[4]; –0.00[10]	–0.08		–0.36	
...	0.10 ± 0.11	–0.3[6]	–0.37		–0.23 ± 0.25	
...	0.10 ± 0.17	0.02[7]	–0.12		–0.28	
...	0.09 ± 0.22	–0.16[9]	–0.09		0.14	
MY Pup	–0.25 ± 0.08	–0.12[1]	–0.12	–0.12[1]	0.10 ± 0.01	0.14[1]
RS Pup	0.07 ± 0.09	0.17[1]; –0.07[3]; –0.12[10]	–0.02 ± 0.22	0.10[1]	–	0.42[1]
RY CMa	–0.12 ± 0.09	0.02[1]	–0.28	–0.30[1]	0.09 ± 0.07	0.16[1]
...	–0.20 ± 0.09		–		–0.01 ± 0.02	
RY Vel	–0.05 ± 0.08	–0.03[1]	–0.22	–0.31[1]	0.31	0.20[1]
RZ CMa	–0.20 ± 0.07		–0.55		–0.08 ± 0.03	
RZ Vel	0.05 ± 0.10	–0.07[1]	–	–0.15[1]	0.29	0.15[1]
ST Vel	–0.14 ± 0.10		–0.34		0.11 ± 0.02	
SW Vel	–0.15 ± 0.08	–0.07[1]; –0.08[2]	–	0.18[1]	–	0.17[1]
SX Vel	–0.18 ± 0.07	–0.03[1]	–0.31	0.12[1]	–0.01	0.05[1]
T Vel	–0.02 ± 0.07	–0.02[1]	–0.02	0.02[1]	0.15 ± 0.01	0.06[1]
TW CMa	–0.51 ± 0.09	–0.18[1]	–	–0.16[1]	–0.15 ± 0.03	–0.03[1]
UX Car	–0.10 ± 0.07		–		0.11 ± 0.01	
V397 Car	–0.08 ± 0.09		–		0.24 ± 0.06	
V Car	–0.06 ± 0.07	–0.04[10]	–0.22 ± 0.16		0.17 ± 0.03	
V Vel	–0.30 ± 0.06		–		–0.34 ± 0.17	
VX Pup	–0.15 ± 0.12	–0.13[1]; –0.70[5]; –0.39[8]	–0.10		0.00 ± 0.03	0.08[1]
VY Car	–0.06 ± 0.06		–		0.15 ± 0.21	
VZ Pup	–0.37 ± 0.07	–0.16[1]	–0.53	–0.10[1]	–0.08 ± 0.01	0.00[1]
WX Pup	–0.15 ± 0.09		–0.36		–0.09	

results show very good agreement with *O* abundances provided by Andrievsky et al. (2004), but with the exception of SX Vel and once again VZ Pup. The ratio [O/Fe] is very close to the abundances provided by Luck & Wepfer (1995) and Kovtyukh et al. (2005). However, oxygen abundances show a higher dispersion when compared with other elements because the lines we used (λ = 6300 Å and 6363 Å) are weak and blended. In order to reduce the intrinsic dispersion we also adopted synthetic spectra, but the improvement was limited, since the wavelength region across these lines is relatively noisy in most of our spectra.

4.3. Sodium

Abundances for sodium cover the range [–0.36 dex–+0.31 dex]. Once again, they agree quite well with previous abundance measurements, and indeed the difference is 0.1 dex or less. Only two stars show a discrepancy of ∼0.15 dex, namely BN Pup and RZ Vel. Most of the Cepheids in our sample are Na−overabundant, a now well-known feature for Galactic supergiants. This Na−overabundance is given by intermediate-mass MS stars, the progenitors of yellow supergiants, by the synthesis of sodium in the Ne − Na cycle in their convective cores. A rotationally induced turbulent and diffusive mixing brings this material enriched in Na into the radiative envelope and shows up at the stellar surface soon after the first dredge up (Sasselov 1986; Denissenkov 1994).

4.4. Aluminium and magnesium

Aluminium and magnesium are both under-abundant in our study, as expected for Galactic supergiants. As far as the Mg is concerned, the comparison is possible only for a few targets, and the abundances we obtained are quite similar to Andrievsky's abundances. On the other hand, the aluminum abundances present a larger discrepancy and current measurements are systematically 0.1–0.2 dex lower than those by Andrievsky and collaborators. This systematic difference only applies to the *Al* abundances, and it could be due to a difference in the atomic parameters chosen for aluminium lines.

Table 5. Aluminium, magnesium, silicon, calcium abundances and comparisons with previous abundance analyses: (1) Andrievsky et al. (2002a).

Object	[Al/H] dex	Others dex	[Mg/H] dex	Others dex	[Si/H] dex	Others dex	[Ca/H] dex	Others dex
AD Pup	–0.22 ± 0.04	0.00[1]	–0.41		–0.04 ± 0.15	–0.19[1]	–0.12 ± 0.08	–0.17[1]
AH Vel	–0.16 ± 0.03		–		0.04 ± 0.16		–0.13 ± 0.12	
...	–0.13 ± 0.04		0.04 ± 0.14		0.09 ± 0.21		–0.06 ± 0.08	
AP Pup	–0.27		0.01		–0.05 ± 0.12		–0.12 ± 0.06	
...	–0.17 ± 0.06		–0.01		0.05 ± 0.14		–0.14 ± 0.04	
...	–0.22 ± 0.20		–		0.03 ± 0.14		–0.13 ± 0.05	
...	–0.24 ± 0.03		–		–0.03 ± 0.15		–	
AQ Car	–0.19 ± 0.05		–		–0.11 ± 0.24		–0.34 ± 0.47	
AQ Pup	–0.29 ± 0.15	0.01[1]	–		–0.06 ± 0.15	–0.10[1]	–0.27 ± 0.16	–0.07[1]
AT Pup	–0.06		–		0.03 ± 0.12		–0.15 ± 0.01	
AX Vel	–0.35 ± 0.04		0.00 ± 0.01		–0.01 ± 0.12		–0.30 ± 0.30	
BG Vel	–0.19 ± 0.02		–0.34		–0.04 ± 0.11		–0.16 ± 0.09	
BN Pup	–0.10 ± 0.03	0.04[1]	–	0.21[1]	0.10 ± 0.18	–0.01[1]	0.05 ± 0.01	0.04[1]
DR Vel	–0.08 ± 0.07		–		0.04 ± 0.08		–0.07	
l Car	–0.15 ± 0.05		–		–0.02 ± 0.06		–0.16	
...	–0.43 ± 0.20		–0.51		–0.16 ± 0.15		–0.27	
...	–0.15 ± 0.06		–		0.00 ± 0.06		–0.08	
...	–0.13 ± 0.06		–		0.01 ± 0.09		–0.14	
MY Pup	–0.25 ± 0.13	0.03[1]	–0.36 ± 0.20	–0.36[1]	–0.02 ± 0.09	–0.08[1]	–0.16 ± 0.09	–0.13[1]
RS Pup	–0.08 ± 0.03	0.17[1]	–		0.08 ± 0.12	0.11[1]	–0.02	0.21[1]
RY CMa	–0.10 ± 0.14		–0.05		–0.04 ± 0.11	0.04[1]	–0.09 ± 0.04	–0.02[1]
...	–0.28 ± 0.04		–0.26		–0.11 ± 0.13		–0.28 ± 0.17	
RY Vel	–0.06 ± 0.07	0.12[1]	–	–0.26[1]	0.06 ± 0.12	0.06[1]	–	–0.11[1]
RZ CMa	–0.31 ± 0.05		–0.17 ± 0.18		–0.14 ± 0.07		–0.22 ± 0.11	
RZ Vel	–0.04	0.04[1]	–	–0.29[1]	0.03 ± 0.12	0.07[1]	–0.13	–0.07[1]
ST Vel	–0.23 ± 0.15		–0.14 ± 0.00		–0.01 ± 0.11		–0.56 ± 0.49	
SW Vel	–0.09 ± 0.25	0.04[1]	–	0.16[1]	–	–0.03[1]	–0.27 ± 0.21	–0.16[1]
SX Vel	–0.16 ± 0.14	0.04[1]	–0.14 ± 0.16	–0.20[1]	0.02 ± 0.19	–0.00[1]	–0.09 ± 0.07	–0.07[1]
T Vel	–0.20 ± 0.11	0.08[1]	–0.26 ± 0.00	–0.24[1]	0.03 ± 0.1	–0.00[1]	–0.06 ± 0.17	–0.02[1]
TW CMa	–0.47 ± 0.13		–0.45 ± 0.00		–0.30 ± 0.14	–0.10[1]	–0.24	–0.19[1]
UX Car	–0.30 ± 0.01		–0.11 ± 0.16		0.01 ± 0.18		0.00 ± 0.01	
V397 Car	–0.23 ± 0.08		–0.20		0.00 ± 0.28		–0.15 ± 0.13	
V Car	–0.24 ± 0.06		–0.28 ± 0.10		0.01 ± 0.25		–0.07 ± 0.13	
V Vel	–0.54 ± 0.12		–0.65 ± 0.30		–0.27 ± 0.06		–0.40 ± 0.07	
VX Pup	–0.33 ± 0.04		–0.18 ± 0.17		–0.10 ± 0.16	–0.06[1]	–0.16 ± 0.06	–0.33[1]
VY Car	–0.16		–0.23 ± 0.00		0.00 ± 0.24		0.03	
VZ Pup	–0.42 ± 0.15	–0.15[1]	–	–0.15[1]	–0.18 ± 0.16	–0.09[1]	–0.35	–0.12[1]
WX Pup	–0.29 ± 0.04		–		–0.04 ± 0.18		–0.21	

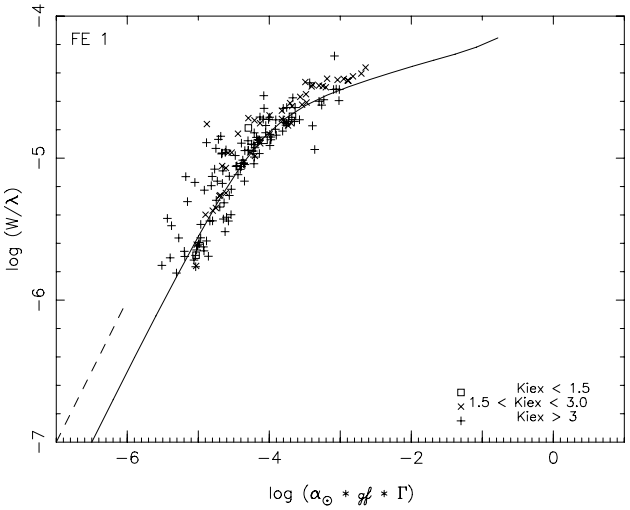

Fig. 3. Observed curve of growth for Fe I in TW CMa. The full line represents the theoretical curve of growth for a typical line (λ = 5000 Å, χ_{ex} = 3). The atmospheric parameters adopted for this star are T_{eff} = 5364 K, log g = 1.0, v_t = 4.0 km s^{-1}, and [Fe/H] = –0.5 dex. The dashed line on the left shows the [Fe/H] = 0 location.

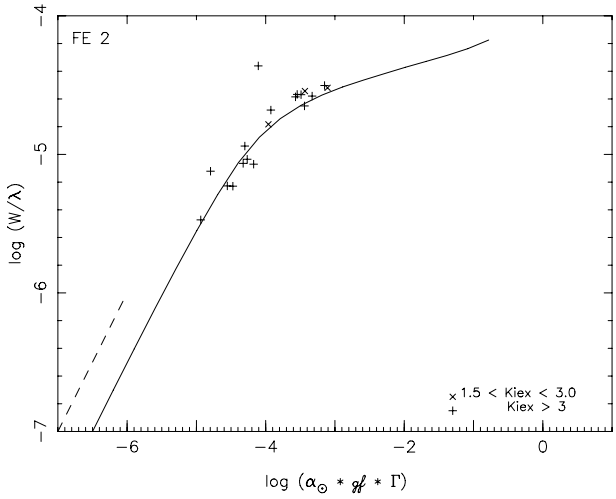

Fig. 4. Observed curve of growth for Fe II in TW CMa. The full line represents the theoretical curve of growth for a typical line (λ = 5000 Å, χ_{ex} = 3). The atmospheric parameters adopted for this star are T_{eff} = 5364 K, log g = 1.0, v_t = 4.0 km s^{-1}, and [Fe/H] = –0.5 dex. The dashed line on the left shows the [Fe/H] = 0 location.

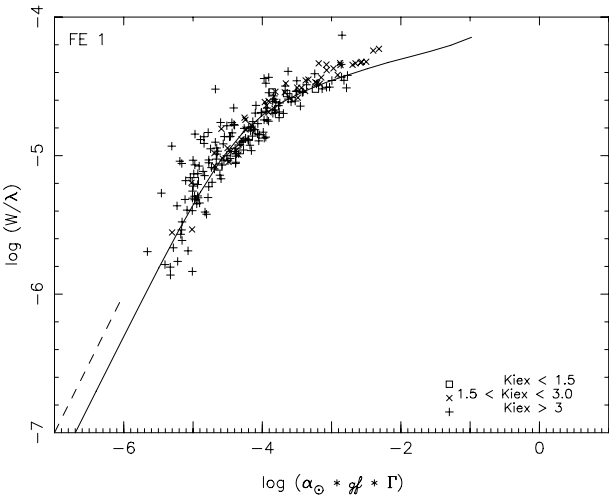

Fig. 5. Observed curve of growth for Fe I in VZPup. The full line represents the theoretical curve of growth for a typical line (λ = 5000 Å, χ_{ex} = 3); the atmospheric parameters adopted for this star are T_{eff} = 5015 K, log g = 0.2, v_t = 4.0 km s^{-1}, and [Fe/H] = –0.3 dex. The dashed line on the left shows the [Fe/H] = 0 location.

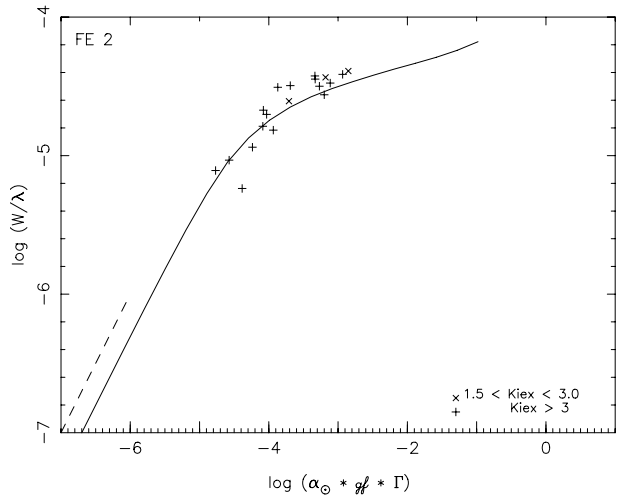

Fig. 6. Observed curve of growth for Fe II in VZPup. The full line represents the theoretical curve of growth for a typical line (λ = 5000 Å, χ_{ex} = 3). The atmospheric parameters adopted for this star are T_{eff} = 5015 K, log g = 0.2, v_t = 4.0 km s^{-1}, and [Fe/H] = –0.3 dex. The dashed line on the left shows the [Fe/H] = 0 location.

4.5. Silicon and calcium

These elements have, as expected, solar-like abundances. Current results agree quite well with the literature values, and indeed the discrepancies are smaller than 0.1 dex, when compared with the measurements provided by Andrievsky and collaborators. In a few cases, the difference is larger, reaching ∼0.2 dex for Si abundances in TW CMa and for Ca abundances in AQ Pup, RS Pup, and VX Pup.

5. Galactic radial abundance gradients

Twarog et al. (1997) suggests that there is a discontinuity in the Galactic chemical abundance gradient in the region located at 10–11 kpc from the Galactic centre. On the other hand, Andrievsky et al. (2004) decided to adopt a multimodal gradient: they divided the range they studied into three regions, namely Zone I: 4.0–6.6 kpc, zone II: 6.6–10.6 kpc, and zone III: 10.6–14.6 kpc. Zone I shows a very steep gradient (–0.128 dex kpc^{-1}), the gradient becomes flatter in Zone II (–0.044 dex kpc^{-1}), while Zone III shows marginal evidence of a radial gradient (+0.004 dex kpc^{-1}). According to these authors, there is a jump in the metallicity gradient in the 10–11 kpc region, where the iron abundance shows a rapid decrease of –0.2 dex. More recent studies based on open clusters support this working hypothesis. In particular, Yong et al. (2005) find that, instead of steadily decreasing with Galactocentric distance, the metallicity reaches a basement metallicity ([Fe/H] ≈ −0.5 dex) beyond 10–12 kpc. This feature is also confirmed by the studies of 3 field red giants (Carney et al. 2005) and of Cepheids (Yong et al. 2006) in the outer disk. However, in the last paper, a sub-sample of Cepheids reaches the basement metallicity at [Fe/H] ≈ 0.9 dex. By using open clusters as chemical composition tracers, Twarog et al. (2006) found a bimodal gradient: the [Fe/H] is close to zero for R_G < 10 kpc, and approximately –0.3 dex for larger Galactocentric distances and with a marginal evidence of chemical composition gradients inside the two zones.

The current Cepheid sample includes only a few targets in the crucial zone, and the use of the abundances estimated by Andrievsky et al. (2002a) and by Mottini et al. (2007) does not allow us to provide sound constraints on the occurrence of a discontinuity in the abundance gradients. Therefore, we decided to adopt a conservative approach by only computing linear gradients. Abundance gradients have then been calculated with a linear regression between abundances and Galactocentric distances for 5 of the 7 elements analysed in this investigation. To compute the goodness-of-fit, we did not adopt the errors listed in Tables 4 and 5 because they only represent the rms of the abundances when we adopt more than one line and not the real measurement errors that come from uncertainties in the determination of the atmospheric parameters.

The measurement errors have been fixed as follow:

- In the case of iron, we assigned them the value of 0.10 dex, since iron abundances have been determined with a sufficient number of lines, and the rms estimates closely match the measurement errors. This value of 0.10 dex, greater than the rms for most of our stars, is therefore slightly overestimated.
- For the other elements, for which the number of lines used ranges from 1 and 5 for a large fraction of the targets, we assigned the value of 0.15 dex to the measurement errors. Such a value is very appropriate for O and Ca, and slightly overestimated for Na.

To improve the sampling across the Galactic disk, we also included 58 Cepheids from the Andrievsky's sample and 11 Cepheids from Mottini et al. (2007) for which NIR photometry is available in the literature. For the former sample both iron and heavy element abundances are available, while for the latter only the iron abundances. The individual distances were estimated using the same approach adopted in Sect. 3.7 and the Galactocentric distances of these additional Cepheids are listed in Table 7. Seven of them are quite distant Cepheids located between 10 and 11.4 kpc, and a few are located toward the Galactic centre, thus extending the baseline we adopt to estimate the gradients. The measurement errors for these objects have been estimated by using the same assumptions we adopted for our sample.

Table 6. Galactic radial abundance gradient in the 8–12 kpc region. The left part of the tables are the values for our sample, the right part includes data from Andrievsky et al. (2002a) and subsequent papers and from Mottini et al. (2007).

Element	slope dex kpc^{-1}	1-σ dex kpc^{-1}	Correlation coeff.	slope dex kpc^{-1}	1-σ dex kpc^{-1}	Correlation coeff.
Fe	–0.061	0.019	0.441	–0.056	0.012	0.410
O	–0.041	0.034	0.226	–0.051	0.022	0.305
Na	–0.042	0.029	0.269	–0.027	0.020	0.199
Si	–0.031	0.029	0.319	–0.044	0.020	0.433
Ca	–0.014	0.029	0.101	–0.024	0.020	0.160

Table 7. Galactocentric distances for Cepheids in Andrievsky et al. (2002a) and following (3 first couples of columns) and in Mottini et al. (2007) (last couple of columns) for which distances based on IR photometry are available.

Object	Distance kpc	Object	Distance kpc	Object	Distance kpc	Object	Distance kpc
SZ Aql	6.96	X Lac	9.01	AV Sgr	6.37	U Car	8.11
TT Aql	7.7	Y Lac	9.08	BB Sgr	7.7	WZ Car	8.14
FM Aql	7.86	Z Lac	9.2	V350 Sgr	7.61	VW Cen	6.83
FN Aql	7.41	BG Lac	8.77	RV Sco	7.74	XX Cen	7.52
V496 Aql	7.63	T Mon	9.75	RY Sco	7.16	KN Cen	6.92
V1162Aql	7.43	SV Mon	10.83	KQ Sco	6.26	GH Lup	7.56
Eta Aql	8.3	CV Mon	10.09	V500 Sco	7.08	S Mus	8.12
V340 Ara	4.99	S Nor	7.73	SS Sct	7.61	UU Mus	7.6
RT Aur	8.94	V340 Nor	6.9	UZ Sct	5.69	U Nor	7.34
SU Cas	8.71	Y Oph	7.93	EW Sct	8.14	LS Pup	11.39
V Cen	7.99	BF Oph	7.68	V367 Sct	6.81	EU Tau	8.87
Del Cep	8.57	GQ Ori	10.84	BQ Ser	7.7		
BG Cru	8.3	X Pup	10.5	ST Tau	9.53		
X Cyg	8.32	S Sge	8.13	SZ Tau	8.96		
VZ Cyg	8.75	U Sgr	7.89	S Vul	7.6		
Beta Dor	8.5	W Sgr	8.08	T Vul	8.34		
W Gem	9.45	Y Sgr	8.02	U Vul	8.16		
RZ Gem	10.66	VY Sgr	6.29	SV Vul	7.8		
AD Gem	11.39	WZ Sgr	6.71				
Zeta Gem	8.86	AP Sgr	7.68				

Table 8. Galactic radial abundance gradient in the 5–12 kpc region. Our sample has been completed with Cepheids from Andrievsky et al. (2002a) and following and from Mottini et al. (2007) for which a homogeneous determination of NIR distances was possible.

Element	slope dex kpc^{-1}	1-σ dex kpc^{-1}	Correlation coeff.
Fe	–0.070	0.008	0.633
O	–0.065	0.013	0.471
Na	–0.071	0.013	0.524
Si	–0.063	0.012	0.666
Ca	–0.062	0.012	0.484

5.1. Iron Galactic radial gradient

We estimated at first the linear Galactic radial gradients for the current Cepheid sample. The slopes, their 1 − σ errors, and the correlation coefficients are listed in Cols. 2–4 of Table 6. Data plotted in the top panel of Fig. 7 show that the slope is –0.061 dex kpc^{-1} in the region ranging from ≈8 to ≈12 kpc. This seems to be a relatively high value when compared with the slopes determined in a similar radial interval by Andrievsky et al. (2002a), who found –0.029 dex kpc^{-1} under the hypothesis of a single-zone gradient, and by Andrievsky et al. (2004): –0.044 dex kpc^{-1} for a multimodal gradient. We note in passing that the correlation coefficient is relatively small (r = 0.447), but quite similar to the correlation coefficient found by Andrievsky et al. (2002a) (r = 0.47).

In order to ascertain on a quantitative basis whether the current slope evaluation is affected by the size of the sample, we also included the Cepheids from Andrievsky's sample (29 Cepheids) and from the Mottini et al. (2007) sample (5 Cepheids) with Galactocentric distances ranging from ∼8 to ∼12 kpc. This means that we doubled the sample size. The results of the linear regression are listed in Cols. 5–7 of Table 6. Interestingly enough, data plotted in the top panel of Fig. 8 show that the new slope, within the 1-σ error, agrees quite well (–0.056 vs. –0.061 dex kpc^{-1}) with the slope only based on the current Cepheid sample. The same outcome applies to the correlation coefficient.

Futhermore, we also decided to check whether current slope evaluations are affected by the Galactocentric radial distances covered by current Cepheid sample. Therefore, we included the entire Andrievsky sample (58 Cepheids) and the entire Mottini et al. (2007) sample (11 Cepheids). This means that we increased the size of the sample by more than a factor of three and by more than 40% the range of Galactocentric distances. The results of the linear regression over the entire sample are listed in Table 8. The top panel of Fig. 9 once again shows that the slope based on the entire data sample agree, within the errors, with those based on a smaller Cepheid sample. However, the 1-σ error is now a factor of two lower (0.008 vs. 0.19); and the correlation coefficient increased by almost the 50%. These findings bring out several circumstantial evidence: *i)* – the slope of the iron radial gradient appears marginally affected by the

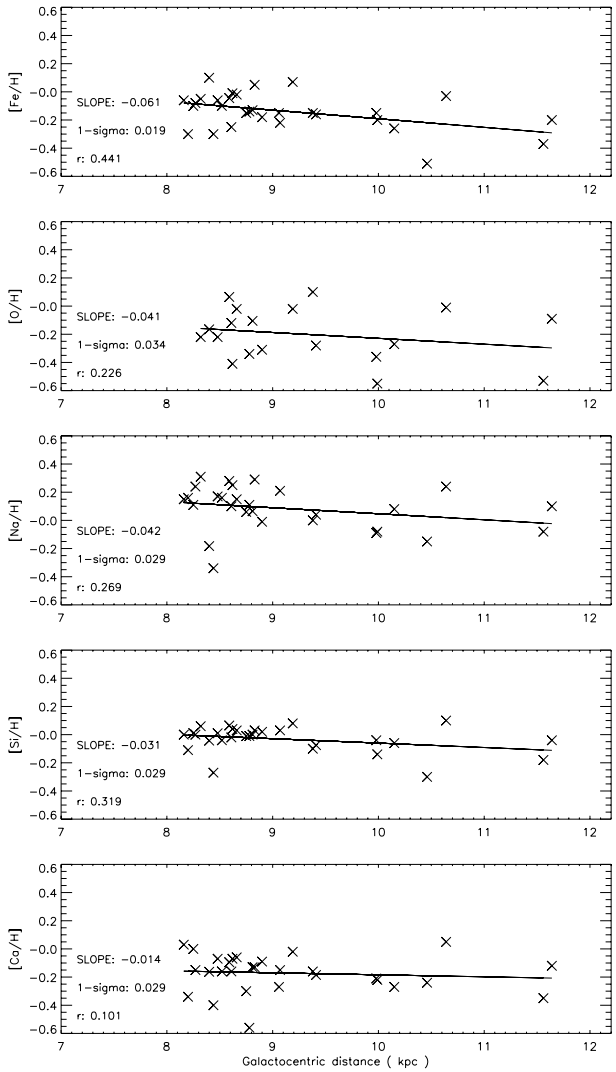

Fig. 7. Galactic radial abundance gradients in the [8–12] kpc region based on our Cepheid sample. The slopes, the $1-\sigma$ errors, and the correlation coefficients are also labelled. The solid line shows the linear regression.

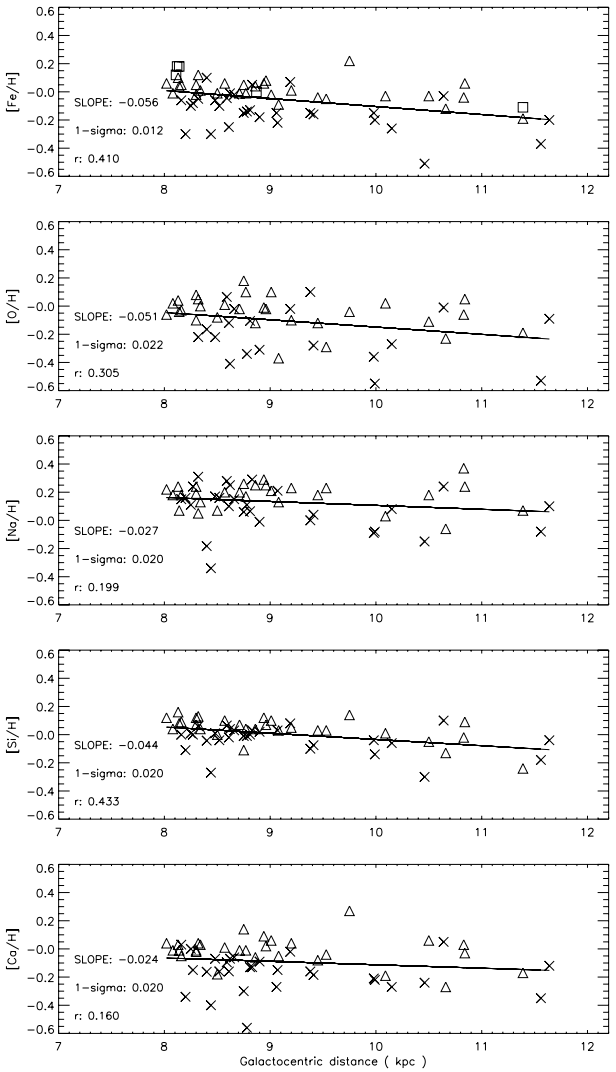

Fig. 8. Galactic radial abundance gradients in the [8–12] kpc region based on our Cepheid sample (crosses) and on data from Andrievsky and collaborators (triangles), and from Mottini et al. (2007) (squares).

uncertainties in radial distances, and indeed the current spread could be due to uncertainties in iron abundances;
ii) – The correlation coefficient depends on the intrinsic accuracy of individual distances, on the range of Galactocentric distances covered by the sample, and to a lesser extent on the spread in metal abundances.
iii) – The slope based over the entire Cepheid sample is marginally affected by the few objects located toward the Galactric centre ($d \leq 6$ kpc) and toward the outer reaches of the Galactic disc ($d \geq 11$ kpc. In fact, we performed a linear regression by removing these objects and both the slope and the $1-\sigma$ error are marginally affected.
iv) – The current iron radial gradient agrees quite well with previous determinations. In particular, Twarog et al. (1997) computed a single-zone gradient using open clusters covering a broad radial interval from 6 to 16 kpc, and they found –0.067 dex kpc^{-1}. The gradient changes to –0.071 dex kpc^{-1} if the cluster BE 21 is included in the sample with a high metallicity value and to –0.076 dex kpc^{-1} if it is included with a low metallicity value. A very similar value (–0.06 dex kpc^{-1}) was also found by Friel et al. (2002) using the same chemical composition tracers. By adopting classical Cepheids, Caputo et al. (2001) found a slope of –0.05 dex kpc^{-1}, which is slightly smaller than the current estimate, but still within the error bars. Our result is also fully consistent with one of the last gradient values determined with Cepheids by Kovtyukh et al. (2005), who added data for 16 distant Cepheids to the Andrievsky's sample. By choosing a single-zone gradient in the 4–15.5 kpc range, they obtained a gradient of –0.06 dex kpc^{-1}. Finally, we can compare our slope with the very recent determination by Luck et al. (2006). They found an iron gradient of –0.068 dex kpc^{-1}, a value that is in remarkable agreement with current estimate. The radial gradients based either on classical Cepheids or on open clusters disagree only with the estimates provided by Kilian-Montenbruck et al. (1994), who found a gradient of -0.003 ± 0.020 dex kpc^{-1}, using B-type stars in the 6–15 kpc region.

5.2. Galactic radial gradient for other elements

Galactic radial abundances gradients for the other elements in the 8–12 kpc region, computed either from current sample or from the sample implemented with Cepheids from the

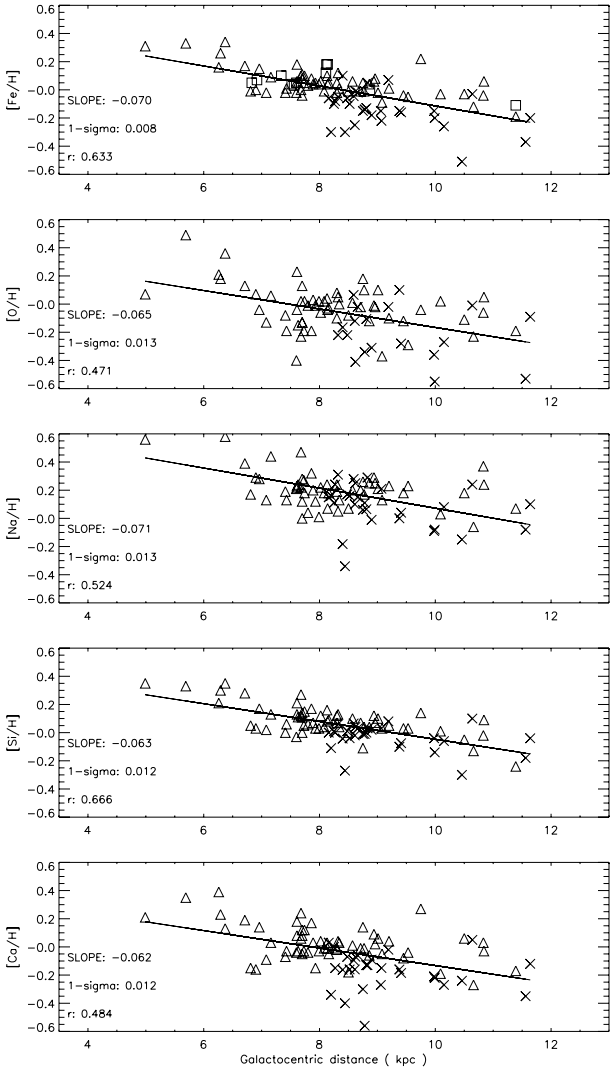

Fig. 9. Same as Fig. 8, but for Cepheids with Galactocentric distances ranging from 5 to 12 kpc.

Andrievsky's sample are once again in good agreement. The discrepancies between the two different slopes are on average of the order of 0.01 dex kpc^{-1}. The only exception is for Na and O, for which the discrepancy is ∼0.015 dex kpc^{-1}, but still within the error bars.

The radial gradients for the other elements in the radial range from 8 to 12 kpc present larger uncertainties when compared with the iron one. A similar trend was also found by Andrievsky et al. (2002a). Once again, current slopes are higher when compared with those estimated by Andrievsky et al. (2002a). In particular, for oxygen they found –0.022 ± 0.009 dex kpc^{-1}, while we find a steeper slope –0.041 ± 0.034 dex kpc^{-1}. The same outcome applies to Na for which they found –0.023 ± 0.006 dex kpc^{-1}, while we find –0.042 ± 0.029 dex kpc^{-1}. On the other hand, the slopes for Si and Ca agree very well, and indeed the slopes are –0.030 ± 0.004 dex kpc^{-1} and –0.021 ± 0.006 dex kpc^{-1}, while we find –0.031 ± 0.029 dex kpc^{-1} and –0.014 ± 0.029 dex kpc^{-1}.

If we compute the radial gradients using the entire Cepheid sample, they appear to be similar to the iron gradient and range from –0.06 to –0.07 dex kpc^{-1}. The gradient appears to be flatter across the solar circle. This behaviour was expected, because it has already been detected, first by Twarog et al. (1997) but also by Andrievsky et al. (2002a). This circumstantial evidence supported the use of a multi-zonal gradient. However, before firm conclusions can be derived, a large sample of homogenous chemical abundances for iron and heavy elements is required.

As far as oxygen is concerned, the comparison with previous studies shows a good agreement with Smartt & Rolleston (1997), Gummersbach et al. (1998), and Rolleston et al. (2000), who found slopes of –0.07 ± 0.01 dex kpc^{-1}, –0.067 ± 0.024 dex kpc^{-1}, and –0.067 ± 0.008 dex kpc^{-1}, using B-type stars as chemical composition tracers. Futhermore, Maciel & Quireza (1998) found –0.058 ± 0.007 dex kpc^{-1} using planetary nebulae and Afflerbach et al. (1997) found –0.064 ± 0.009 dex kpc^{-1} from HII regions. However, current results do not support the flat slopes for the oxygen radial gradient found by Fitzsimmons et al. (1992) (–0.03 ± 0.02 dex kpc^{-1}) and Kilian-Montenbruck et al. (1994) (–0.021 ± 0.012 dex kpc^{-1}) using B-type stars or by Deharveng et al. (2000) (–0.0391 ± 0.005 dex kpc^{-1}) using HII regions. Obviously they also do not agree with the null radial gradient found by Kaufer et al. (1994) (–0.000 ± 0.009 dex kpc^{-1}) using B-type stars.

For silicon, our results are in good agreement with Rolleston et al. (2000), who found a slope of –0.06 ± 0.01 dex kpc^{-1}, but agree neither with the flatter slopes by Kilian-Montenbruck et al. (1994) (+0.000 ± 0.018 dex kpc^{-1}) nor with the steeper slopes by (Gummersbach et al. 1998) (–0.107 ± 0.028 dex kpc^{-1}). Both these authors were using B-type stars.

However, in order to ascertain whether the difference in the different slope estimates are dominated by deceptive empirical uncertainties or they might be intrinsic, a detailed investigation of stellar ages and radial distribution of the different chemical tracers is required.

6. Conclusions

We have determined the abundances of iron and six light metals (O, Na, Mg, Al, Si, Ca) in 30 Galactic Cepheids. These abundances were used to compute a slope for the Galactic radial abundance gradient. For the iron Galactic gradient in the radial distance range from 8 to 12 kpc we found slopes of –0.061 dex kpc^{-1} and of –0.056 dex kpc^{-1} if we include 69 Cepheids with homogeneous distance determinations. The current slope is steeper when compared with the slope estimated by Andrievsky et al. (2002a) for the central region of the multi-zonal gradient. On the other hand, the current gradient computed over a more extended baseline (–0.070 ± 0.008 dex kpc^{-1}) is fully consistent with other studies based either on open clusters or on Cepheids. Current findings do not allow us to provide firm constraints on the multi-modal model, due to the limited number of targets in the crucial zone. The hypothesis of a multi-modal gradient deserves further investigations, mainly to fill the transition region across 10–11 kpc.

Acknowledgements. This research made use of the SIMBAD and VIZIER databases, operated at the CDS, Strasbourg, France. We would also to thank A.M. Piersimoni for help in estimating the mean NIR magnitudes based on 2MASS photometry. We deeply thank F. Pont and F. Kienzle who did the observations.

References

Afflerbach, A., Churchwell, E., & Werner, M. W. 1997, ApJ, 478, 190
Andrievsky, S. M., Kovtyukh, V. V., Usenko, I. A., Klochkova, V. G., & Galazutdinov, G. A. 1994, A&AS, 108, 433
Andrievsky, S. M., Kovtyukh, V. V., Luck, R. E., et al. 2002a, A&A, 381, 32

Andrievsky, S. M., Bersier, D., Kovtyukh, V. V., et al. 2002b, A&A, 384, 140
Andrievsky, S. M., Kovtyukh, V. V., Luck, R. E., et al. 2002c, A&A, 392, 491
Andrievsky, S. M., Luck, R. E., Martin, P., & Lépine, J. R. D. 2004, A&A, 413, 159
Barrell, S. L. 1982, MNRAS, 200, 127
Berdnikov, L. N., Dambis, A. K., & Vozyakova, O. V. 2000, A&AS, 143, 211
Bono, G., Caputo, F., Castellani, V., & Marconi, M. 1999, ApJ, 512, 711
Boyarchuk, A. A., & Lyubimkov, L. S. 1984, Afz, 20, 85
Caputo, F., Marconi, M., Musella, I., & Pont, F. 2001, A&A, 372, 544
Cardelli, J. A., Clayton, G. C., & Mathis, J. S. 1989, ApJ, 345, 245
Carney, B. W., Yong, D., & de Almeida, M. L. T. 2005, AJ, 130, 1111
Charbonneau, P. 1995, ApJS, 101, 309
Chiappini, C., Matteucci, F., & Romano, D. 2001, ApJ, 554, 1044
Clementini, G., Carretta, E., Gratton, R., et al. 1995, AJ, 110, 2319
Deharveng, L., Peña, M., Caplan, J., & Costero, R. 2000, MNRAS, 311, 329
Denissenkov, P. A. 1994, A&A, 287, 113
Feast, M., & Whitelock, P. 1997, MNRAS, 291, 683
Fernie, J. D., Beattie, B., Evans, N. R., & Seager, S. 1995, IBVS, N4148
Fitzsimmons, A., Dufton, P. L., & Rolleston, W. R. J. 1992, MNRAS, 259, 489
Friel, E. D., Janes, K. A., Tavarez, M., et al. 2002, AJ, 124, 2693
Fry, A. M., & Carney, B. W. 1997, AJ, 113, 1073
Kaufer, A., Szeifert, T., Krenzin, R., Baschek, B., & Olf, B. 1994, A&A, 289, 740
Kerr, F., & Lynden-Bell, D. 1986, MNRAS, 221, 1023
Kilian-Montenbruck, J., Gehren, T., & Nissen, P. E. 1994, A&A, 291, 757
Kiss, L. L., & Vinko, J. 2000, MNRAS, 314, 420
Grevesse, N., Noels, A., & Sauval, J. 1996, ASPC, 99, 117
Gummersbach, C. A., Kaufer, D. R., Schäfer, D. R., Szeifert, T., & Wolf, B. 1998, A&A, 338, 881
Gustafsson, B., Bell, R. A., Eriksson, K., & Nordlund, Å. 1975, A&A, 42, 407
Kovtyukh, V. V., & Gorlova, N. I. 2000, A&A, 358, 587
Kovtyukh, V. V., Andrievsky, S. M., Usenko, I. A., & Klochkova, V. G. 1996, A&A, 316, 155
Kovtyukh, V. V., Wallerstein, G., & Andrievsky, S. M. 2005, PASP, 117, 1173
Kupka, F., Piskunov, N. E., Ryabchikova, T. A., Stempels, H. C., & Weiss, W. W. 1999, A&AS, 138, 119
Laney, C. D., & Stobie, R. S. 1994, MNRAS, 266, 441
Luck, R. E., & Lambert, D. L. 1981, ApJ, 245, 1018
Luck, R. E., & Lambert, D. L. 1985, ApJ, 298, 782
Luck, R. E., & Bond, H. E. 1989, ApJS, 71, 558
Luck, R. E., & Lambert, D. L. 1992, ApJS, 79, 303
Luck, R. E., & Wepfer, G. G. 1995, AJ, 110, 2425
Luck, R. E., Gieren, W. P., Andrievsky, S. M., et al. 2003, A&A, 401, 939
Luck, R.E., Kovtyukh, V. V., & Andrievsky, S. M. 2006, AJ, 132, 902
Maciel, W. J., & Quireza, C. 1999, A&A, 345, 629
Maciel, W. J., Costa, R. D. D., & Uchida, M. M. M. 2003, A&A, 397, 667
Mottini, M., Primas, F., Romaniello, M., Bono, G., Groenewegen, M. A. T., François, P. 2007, A&A, accepted
Neese, C. L., & Yoss, K. M. 1988, AJ, 95, 463
Persson, S. E., Madore, B. F., Krzemiński, W., et al. 2004, AJ, 128, 2239
Rolleston, W. R. J., Smartt, S. J., Dufton, P. L., & Ryans, R. S. I. 2000, A&A, 363, 537
Ryabchikova, T. A., Piskunov, N. E., Stempels, H. C., Kupka, F., & Weiss, W. W. 1999, Proc. of the 6th International Colloquium on Atomic Spectra and Oscillator Strengths, Victoria BC, Canada, 1998, Phys. Scr., T83, 162
Sasselov, D. D. 1986, PASP, 98, 561
Schaller, G., Shaerer, D., Meynet, G., & Maeder, A. 1992, A&AS, 96, 269
Smartt, S. J., & Rolleston, W. R. J. 1997, ApJ, 481, L47
Soszyński, I., Gieren, W., & Pietrzyński, G. 2005, PASP, 117, 823
Spite, M. 1967, Ann. Astrophys., 30, 211
Thévenin, F. 1998, Bull. CDS 49, Catalogue III/193
Twarog, B. A., Ashman, K. M., & Antony-Twarog, B. J. 1997, AJ, 114, 2556
Twarog, et al. 2006, AJ, submitted
Yong, D., Carney, B. W., & de Almeida, M. L. T. 2005, AJ, 130, 597
Yong, D., Carney, B. W., de Almeida, M. L. T., & Pohl, B. L. 2006, AJ, 131, 2256